The International Journal of Advanced Manufacturing Technology (2018) 99:1967–1977
https://doi.org/10.1007/s00170-018-2614-5

ORIGINAL ARTICLE

U-R relationship prediction method for aluminum alloy circular tube free-bending process based on sensitivity analysis of material parameters

Xunzhong Guo[1] · Hao Xiong[1] · Yong Xu[2,3] · Ali Abd El-Aty[2] · Yannan Ma[1] · Yonghao Zhao[3] · Shihong Zhang[2]

Received: 24 May 2018 / Accepted: 16 August 2018 / Published online: 30 August 2018

Abstract
The bending radius (R) of the bending component is defined by the deflection (U) of the bending die in the tube free-bending process. The *U-R* relationship is the key factor to obtain the precise geometry size of the complex bending tubular components. Therefore, this study aims at proposing a new method to predict the *U-R* relationship for the arbitrary power hardening aluminum alloy (Al alloy) circular tube based on the *U-R* relationship of the reference material and the sensitivity analysis of material parameters, which may reduce many experimental works. In the current study, AA1100 alloy was set as the reference material, and the effects of each material parameter on the *U-R* relationship were investigated by carrying out the deformation and sensitivity analysis of the FEA simulation results. The results show that the bending radius increases with the decrease of elastic modulus (E), density (ρ), and strain-hardening exponent (n) and the increase of strength coefficient (K) and initial yield stress (σ_s), where σ_s has the greatest influence on the *U-R* relationship. Moreover, the *U-R* relationship prediction method for arbitrary power hardening Al alloy circular tube was presented based on the sensitivity analysis of the reference material. Finally, the bending tests of the AA6061-T6 tubes were carried out to prove the accuracy of the *U-R* relationship prediction method. The bending results show that the experimental *U-R* relationship of the AA6061-T6 tube was consistent with the predicted value, and the prediction method had good applicability to power hardening Al alloy circular tube.

Keywords Free bending · Material parameters · *U-R* relationship · Sensitivity analysis · Power hardening aluminum alloy · Prediction method

1 Introduction

As a new bending technique, the free-bending technology has great potential [1] and can achieve complex bending geometries without changing the die [2] and reclamping the tube [3]. In the free-bending process, the bending radius can be changed arbitrarily by shifting the bending die to certain positions, and the resulting bending geometry shows only small cross section deformations and low reduction of the wall thickness in the outer bend after bending due to the bending die built like a sliding bushing and the applied pushing force [4].

The *U-R* relationship (deflection of bending die-bending radius) is a crucial factor for the forming accuracy of the tube free-bending process. The material properties are the most important factor affecting the *U-R* relationship in case of the same cross section of the tube. The bending radius (R) of different materials varies even though the deflection (U) does not change [5]. Therefore, the *U-R* relationship should be revised based on the theoretical calculations according to the material property of the tube [6]. Due to the diversity of materials, in-process production, there is only one corresponding *U-R* relationship for each alloy and the bending tests need to

✉ Yong Xu
yxu@imr.ac.cn

[1] College of Material Science and Technology, Nanjing University of Aeronautics and Astronautics, Nanjing 211100, People's Republic of China

[2] Institute of Metal Research, Chinese Academy of Sciences, Shenyang 110016, People's Republic of China

[3] Nano and Heterogeneous Materials Center, School of Materials Science and Engineering, Nanjing University of Science and Technology, Nanjing 210094, People's Republic of China

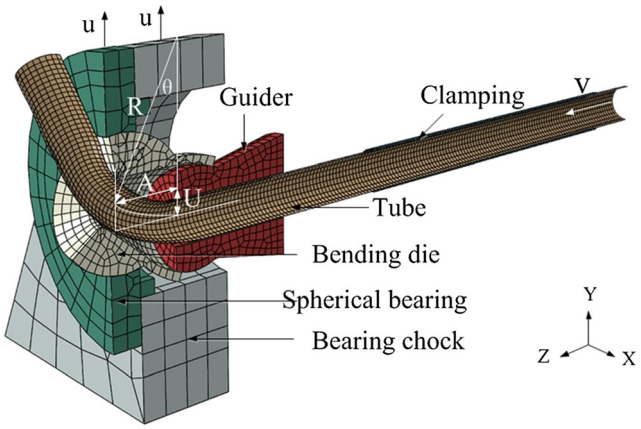

Fig. 1 FE model of three-axis free bending

be accomplished several times for the specific alloy until the bending results match the target geometry [7]. A large number of early bending tests led to lower production efficiency and increased the costs of free-bending production. Therefore, it is vital to find a new methodology to quickly establish the *U-R* relationship for the arbitrary alloy circular tube to cut the work of bending tests.

To date, few investigations were accomplished on the effect of material parameters on *U-R* relationship of tubes in the free-bending process. Gantner put forward the theoretical relationship between the deflection (*U*) of the bending die and the bending radius (*R*) by presenting the free-bending kinematic and mathematical models [8]. Gantner also mentioned that appropriate settings must be made for each type of material being bent due to the variation in the springback behavior of the different materials [9]. Murata found that bending radii and bending forces are affected by the tube material by carrying out bending tests for three different alloys (aluminum alloy, brass, and copper) [4]. Ma obtained the *U-R* relationship of copper T2 by setting different deflections of the bending die in the finite element (FE) model of the free-bending process [10]. Guo conducted bending experiments based on the research results to prove the reliability of *U-R* relationship which is obtained from FE modeling [11]. The result revealed that dimensions of the bent spatial tube were close to the CAD model and the deviation of the bending radius and bending angle was supposed to occur due to springback after deformation. The existing investigations only aimed to obtain the *U-R* relationship of one or more specific materials through experiments or simulations and did not explain the influence of the material's internal factors on the *U-R* relationship. However, the influence of material factors on the *U-R* relationship is of great practical significance for understanding the forming mechanism of free bending and even realizing the prediction of the *U-R* relationship for the arbitrary material.

Accordingly, in this study, a new method to establish the *U-R* relationship of the arbitrary target power hardening Al alloy circular tube quickly is proposed by analyzing the effect of material parameters on the *U-R* relationship. The predicted *U-R* relationship has good agreement with the *U-R* relationship obtained from experimentation, which could be used in the bending program of the target bending part directly. The process of predicting the *U-R* relationship was divided into three steps in the current study. Firstly, deformation analysis of each basic material parameter on bending radius was conducted by ABAQUS/explicit FE code. Moreover, the sensitivity analysis model was established to investigate the influence of material parameters on the *U-R* relationship in the free-bending process based on the multiparameter sensitivity analysis method. Finally, based on the deformation analysis and sensitivity analysis, the effect as well as the sensitivity factor of the material parameters, such as Young's modulus and yield strength, on the bending radius could be obtained, and the *U-R* relationship of the target power hardening Al alloy circular tube could be forecasted by calculating the deviation of the bending radius caused by the variation of each influential material parameters.

2 Free-bending FEA model

1100 aluminum alloy (AA1100) tubes with specifications of 15 mm (D_0) × 1 mm (t) were utilized as the basic research object, and the ABAQUS/explicit FE code was used to

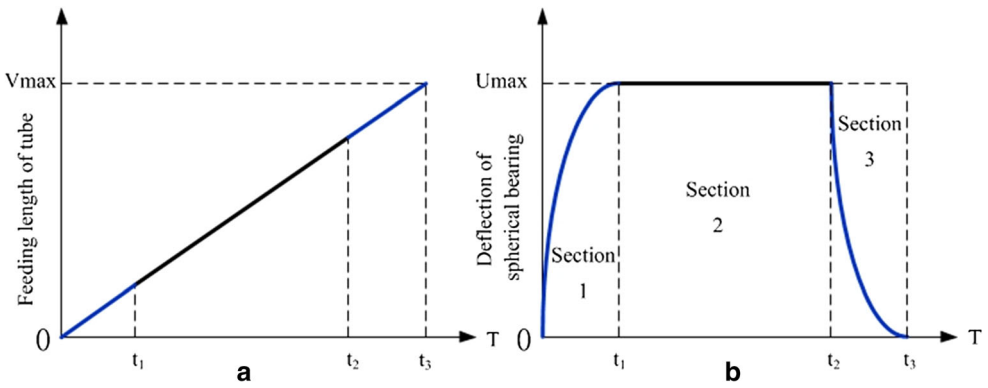

Fig. 2 Motion curve of time displacement: **a** feed of the tube; **b** deflection of the spherical bearing

Table 1 Material parameters of the AA1100 tube

Density ρ (kg/m^3)	Young's modulus E (GPa)	Yield strength σ_s (MPa)	Work-hardening exponent n	Intensity coefficient K (MPa)	Poisson's ratio u
2.67	62.10	250.51	0.098	402.96	0.33

conduct the numerical simulation of the forming process, as shown in Fig. 1. Spherical bearings, guider, and clamping were defined as discrete rigid bodies with R3D4 element type, and the bending die was dispersed into C3D8R solid elements. The tube was set to a deformable shell with a grid type of S4R. The analysis step was adjusted to dynamic explicit and the interaction was set to general contact. The guider and clamping were set to encastre. The end of the tube was set a specified movement speed along the axis (Z direction), while the bending die was not set load. The spherical bearing and bearing chock were set the same movement, respectively, in the Y direction, of which the motion curve is shown in Fig. 2. The calculation of the motion curve is as shown in Eqs. (1) to (7).

For the free-bending forming process, the forming of any bend usually has three stages, as depicted in Fig. 2b. In stage 1, the spherical bearing moves from the origin position to a deflection position and the translation and rotation of the bending die is held as long as the deflection increases correspondingly; at its end time, the bending die reaches the maximal position and an arc has been formed which is a part of the entire bend. In stage 2, the deflection keeps in the maximal position to form or complete the rest of the bend with a constant value of U_{max} which is determined by the required radius R. At the same time, the tube is kept feeding till the required bending angle is completed. In stage 3, the deflection of the bending die decreases to its end position; at its start time, the tube has already the required radius (R) and bending angle (θ) and the feed tube is not bent in this section.

$$V = v \times t \tag{1}$$

$$\text{Stage 1}: U = R - R\cos\frac{vt}{R} + \tan\frac{vt}{R}\left(A - R\sin\frac{vt}{R}\right) \tag{2}$$

$$t_1 = \frac{\pi \times R \times \arcsin A/R}{180 \times V} \quad (0 \le t \le t_1) \tag{3}$$

$$\text{Stage 2}: U = R - R\cos\frac{vt}{R} + \tan\frac{vt1}{R}\left(A - R\sin\frac{vt}{R}\right) \tag{4}$$

$$t_2 = \frac{\pi \times R \times \theta}{180 \times V} \quad (0 \le t \le t_2 - t_1) \tag{5}$$

$$\text{Stage 3}: U = R - R\sqrt{1 - \left(\frac{A - vt}{R}\right)^2} \tag{6}$$

$$t_3 = t_2 + A/v \quad (0 \le t \le t_3 - t_2) \tag{7}$$

The basic mechanical and physical properties of the AA1100 tube are shown in Table 1. The power hardening elastic-plastic model ($\sigma = K\varepsilon^n$) [12] was selected as the constitutive equation of the plastic section of the AA1100 tube. Young's modulus (E), yield strength (σ_s), work-hardening exponent (n), and intensity coefficient (K) of the AA1100 tube were obtained by stress-strain data fitting through uniaxial tensile test (Fig. 3). The Poisson's ratio (u) was measured by the combination of uniaxial tension and torsion tests with various extensometers to obtain longitudinal and lateral strain data. The density (ρ) was measured through the hydrometer method.

The tube feeding speed (v) was assumed to be 10 mm/s. The distance (A) between the outlet of the bending die and guider was set as 22.5 mm ($1.5D_0$). The clearance between the tube and tools was all set as 0.1 mm. Since the bending die and the guider are carbide tools, the lubrication unit was designed

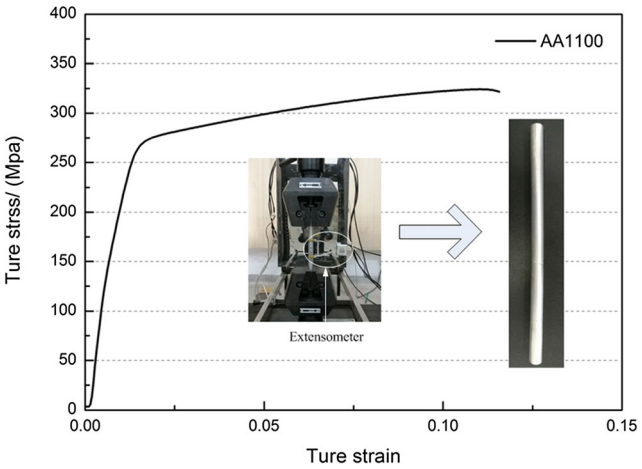

Fig. 3 True stress-strain curve of the AA1100 tube obtained through uniaxial tensile test

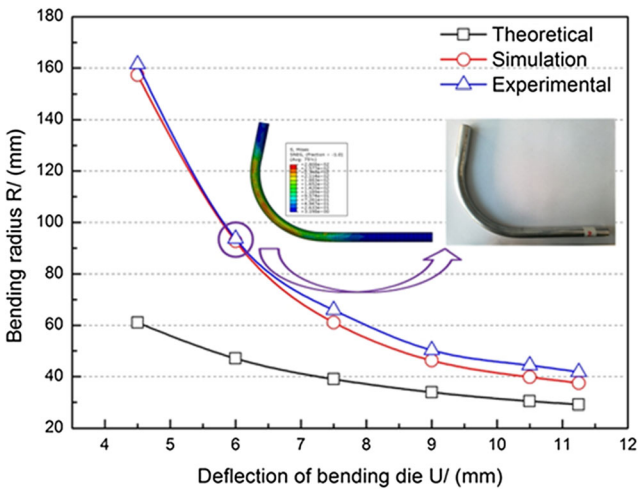

Fig. 4 *U-R* relationship of the AA1100 tube

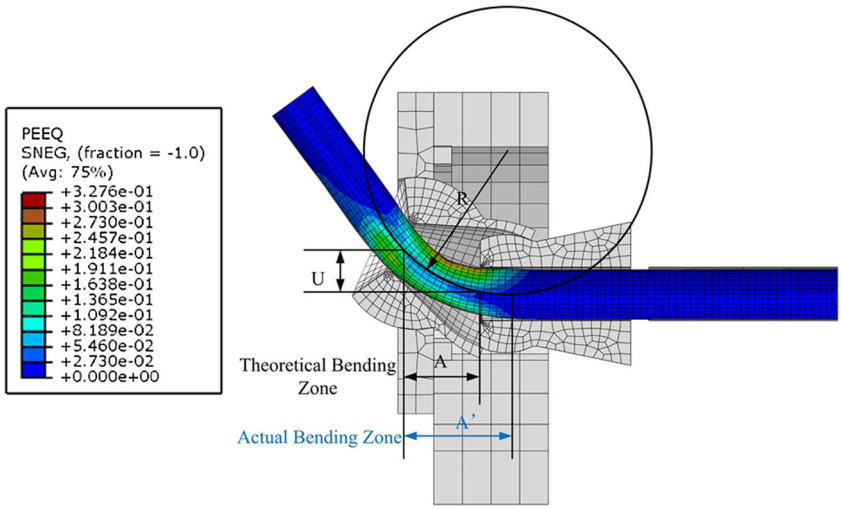

Fig. 5 Enlargement of the actual bending deformation zone

near the bending die. For an evenly applied lubrication film, the coefficient of friction between the tools and the tube was very low. The coefficient of friction between the tools and the Al alloy tube in the FE model was assumed to be 0.06 [13].

In order to validate the reliability of the FE model, the simulation and bending test under different deflections (U) of the bending die were carried out. The comparison between the U-R relationship of simulation results, bending results, and the theoretical values is depicted in Fig. 4. Due to the variation in the actual deformation zone, springback behavior, and deformation of the cross section of the different materials, the bending radius was not equal to the theoretical value (Eq. (8)) and not constant for different materials [14]. The variation trend of the bending radius under different deflections of the bending die was in agreement with the theoretical curve.

$$R = \frac{A^2 + U^2}{2U} \tag{8}$$

The determination of theoretical values was based on a variety of assumptions. The most influential assumption is that the bending zone was defined only between the guider's outlet radius and the feed-through of the bending die. The axial length of the bending zone is equal to the (A) value. However, whether in finite element simulation or practical bending test, the tube in the area near the outlet of the guider will not remain straight during the bending process, and thus the length of the bending zone (A) would be expanded, as shown in Fig. 5. Therefore, under the same deflection of the bending die, the actual bending radius will be greater than the theoretical results. The deviation was more obvious when the deflection of the bending die was relatively small.

As suggested by Fig. 6, the maximum relative error of the results of simulation and bending test was about 10%. Therefore, the FE model established in this study could be used as a system model to conduct the sensitivity analysis on bending radius in the free-bending process of aluminum alloy circular tubes.

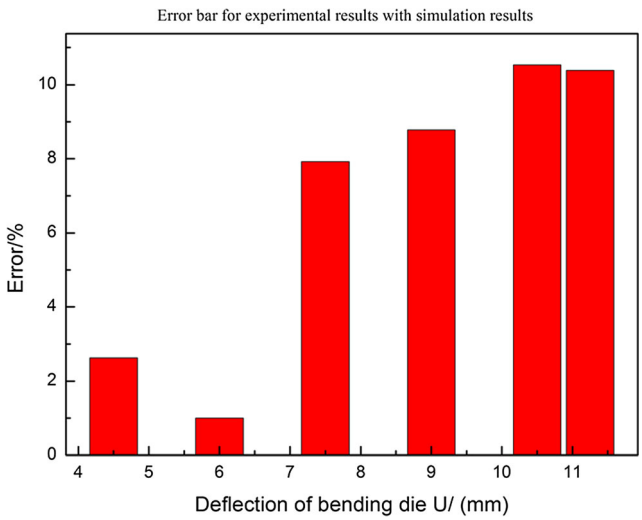

Fig. 6 Error bar for experimental results compared with simulation results

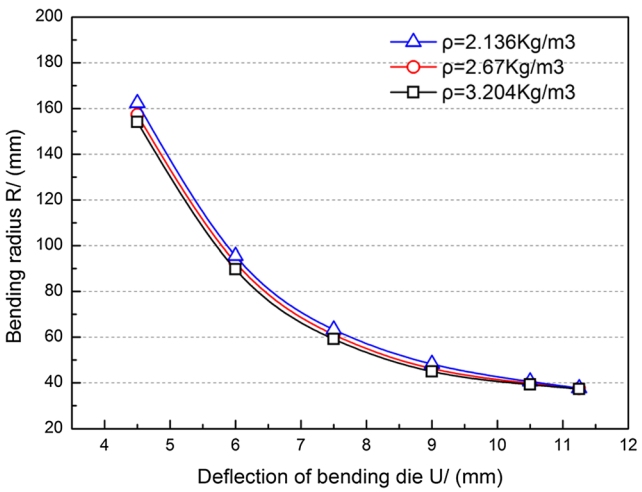

Fig. 7 Effect of density on U-R relationship

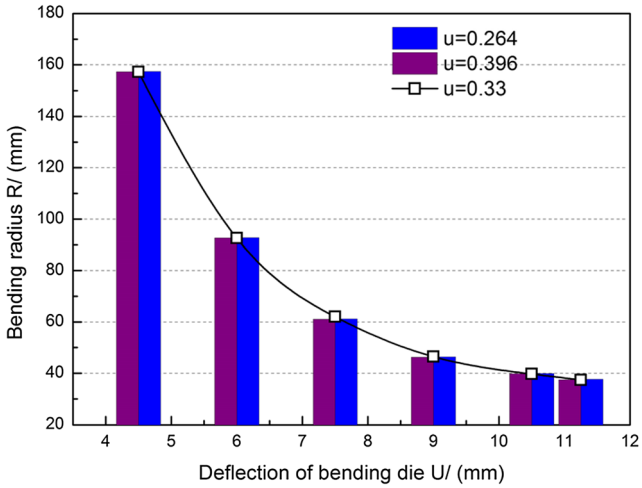

Fig. 8 Effect of Poisson's ratio on *U-R* relationship

3 Deformation analysis

Using the FE model to change each material in turn, while keeping the other parameters constant, the effect of each material parameter on the *U-R* relationship could be obtained.

3.1 Density and Poisson's ratio

Figures 7 and 8 show the *U-R* relationship of the AA1100 tube with different densities and Poisson's ratios, respectively. It can be found that no matter what the deflection of the bending die is, the material density has little effect on the bending radius, especially under conditions of small bending radius. The small variation of the bending radius may be related to the inertia. The bigger the density, the bigger the inertia, and the easier the tube is bent and shaped. Tangential deformation and radial deformation occur mainly in the tube bending process, and the tube is hardly influenced by the circumferential deformation [15]. Poisson's ratio is only related to the horizontal deformation of the tube. Thus, it does not affect the bending radius and *U-R* relationship.

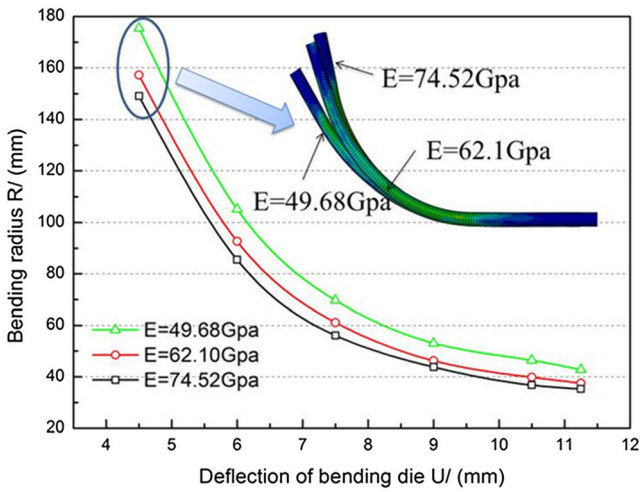

Fig. 9 Effect of Young's modulus on *U-R* relationship

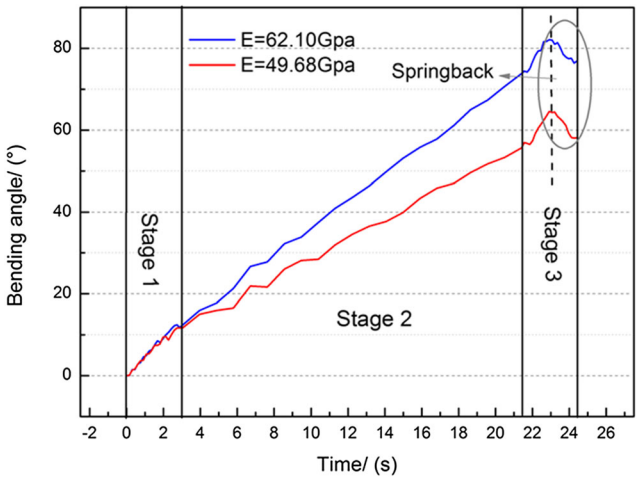

Fig. 10 Effect of Young's modulus on bending angle

3.2 Young's modulus

The *U-R* relationship of the AA1100 tube with different Young's moduli is depicted in Fig. 9. It can be found that no matter what the deflection of the bending die is, the bending radius decreases with the increase of the Young's modulus of the tube. The greater the Young's modulus, the smaller the Young's modulus has an effect on the bending radius. Therefore, it is difficult to increase the Young's modulus infinitely for the purpose of reducing the bending radius to an infinitely small size.

The curve of variation of bending angle with different Young's moduli is shown in Fig. 10. In stage 1, the Young's modulus change has little effect on the bending radius and bending angle. The elastic deformation stage and the plastic deformation stage in stage 1 bending process are shown in Fig. 11. It can be found that the larger the Young's modulus, the greater the amount of elastic deformation at the initial stage of the tube bending process, but this increase is negligible compared to the total amount of bending deformation. Therefore, at the end of stage 1, the tube undergoes complete plastic deformation, and the total amount of deformation of the tubes with different Young's moduli shows a very small difference.

In stage 2, the difference of the bending angle of the tube caused by the variation of Young's modulus increases with the feeding time of the tube. At the start of stage 3, the intrados of the tube is subjected to the bending die, since the bending shape is deviated from the theoretical state. The bending process is going on and bending angle increases continuously. Then as the bending die is returned to a certain position and no longer exerts force on the bent tube, the bending angle is decreased due to the springback behavior, since there is no load from any die. The amount of springback depends on

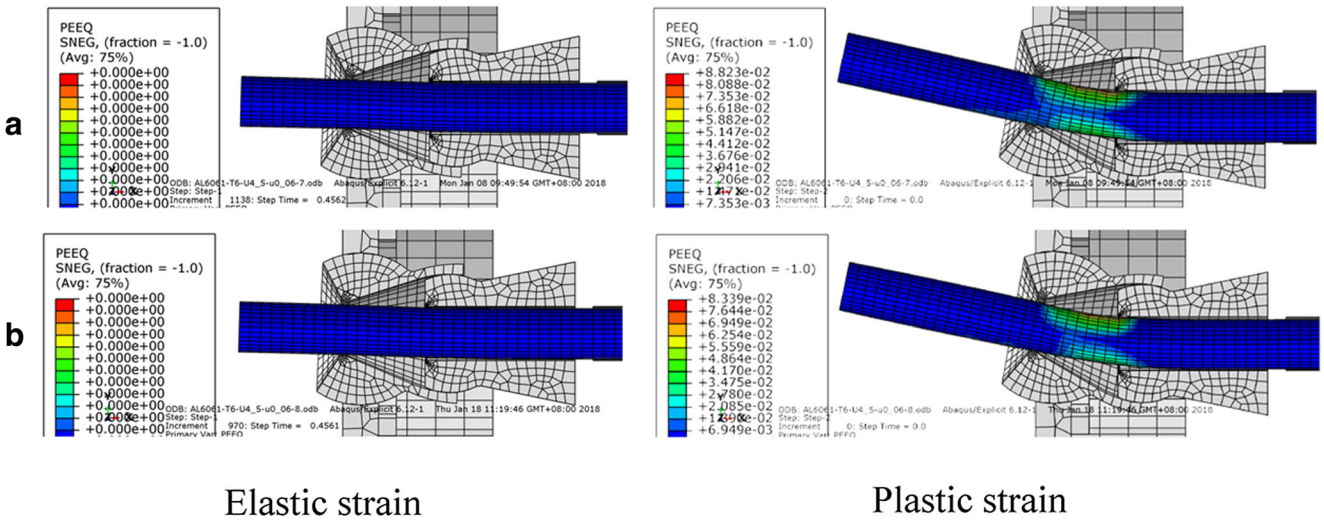

Fig. 11 Effect of Young's modulus on elastic and plastic strain in section 1: **a** $E = 62.1$ GPa; **b** $E = 49.68$ GPa

the elastic deformation of the bent tubes. Young's modulus is an important material parameter used to measure the capacity to resist the elastic deformation [16], so it greatly influences the amount of springback. The springback angle of the bent tube ($E = 62.1$ GPa) is 5.72°, while the springback angle of the bent tube ($E = 49.68$ GPa) is 6.47°. It is found that the tube with smaller Young's modulus has a larger springback angle because the high ratio of yield strength to Young's modulus may induce significant elastic recovery after unloading [17]. In conclusion, tubes with larger Young's modulus bend more at the same tube feeding time, so the bending radius of a tube is smaller than that with larger Young's modulus.

3.3 Initial yield strength

The *U-R* relationship of the AA1100 tube with different initial yield strengths is shown in Fig. 12. It can be found that with the same deflection of the bending die, the bending radius increases with the increase of the initial yield strength of the tube. This is because the tube of low yield strength has better cold forming ability and easier to be bent. However, small initial yield strength may lead to intrados wall collapse in the bending deformation zone when the deflection of the bending die is relatively large, as depicted in Fig. 13.

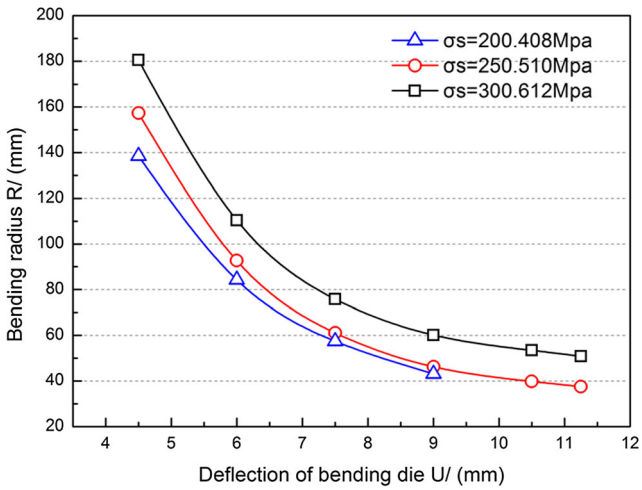

Fig. 12 Effect of initial yield strength on *U-R* relationship

3.4 Strength coefficient (*K*) and work-hardening exponent (*n*)

Five stress-strain curves with different values of *K* and *n* are shown in Fig. 14, where the black dashed line is the original true stress-strain curve of AA1100. By respectively making the value of *K* and *n* fluctuate by 20% in the original value, the remaining four curves have also been obtained. The *U-R* relationship obtained from the above five sets of stress-strain data is shown in Fig. 15. It can be drawn that the bending radius increases with the increase of strength coefficient and decrease of work-hardening exponent of the tube in case of the same deflection of the bending die. Within the same range of variation, strength coefficient has a greater effect on the bending radius than the work-hardening exponent. According to the trends in the curve point of view, the limit bending radius of AA1100 with different strength coefficients and work-hardening exponents is about $2.5D_0$ ($D_0 = 15$ mm).

4 Sensitivity analysis

4.1 Multiparameter sensitivity analysis method

Multiparameter sensitivity analysis method is a method of analyzing the system stability in system analysis [18]. When the multiparameter sensitivity analysis is carried out, it only changes the value of one parameter and keeps the other parameters' benchmark value constant. Therefore, the increment

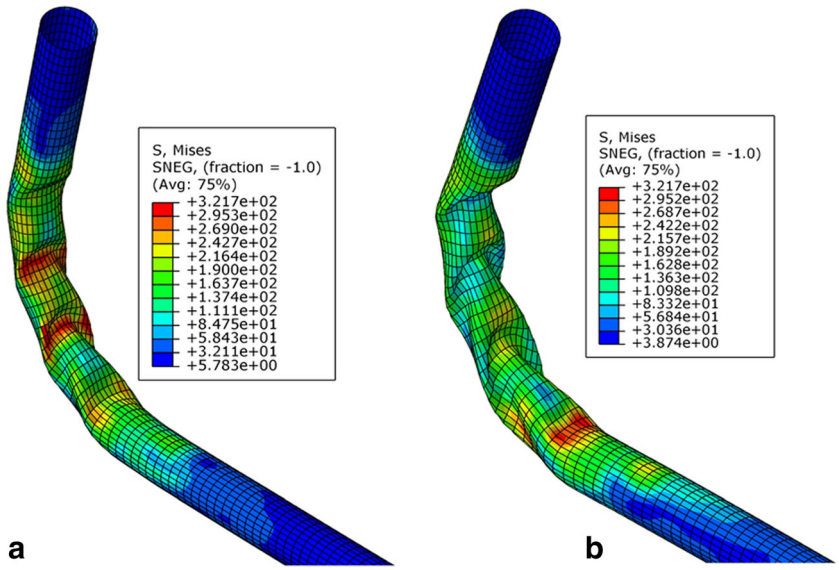

Fig. 13 Tube intrados wall collapse ($\sigma_s = 200.408$ MPa): **a** $U = 10.5$ mm; **b** $U = 11.25$ mm

and the influence rate of the safety factor caused by the unit value of each influence factor are sequentially calculated. It is assumed that the system's system characteristics (P) are mainly determined by n parameters:

$$P = f(\alpha_1, \alpha_2, \alpha_3, \ldots\ldots\ldots\ldots\ldots\alpha_n) \tag{9}$$

When the n parameters are all at the base value, the system feature is the benchmark state (P^*). ($\alpha_k{}^*$) is the reference state values for the factor (α_k).

$$P^* = f\left(\alpha_1{}^*, \alpha_2{}^*, \alpha_3{}^*, \ldots\ldots\ldots\ldots\ldots\alpha_n{}^*\right) \tag{10}$$

In the actual systems, the parameters determining system characteristics are often different physical quantities, and their units are different. Therefore, dimensionless processing is required to realize the sensitivity analysis of those parameters. The relative errors (δ_P, $\delta\alpha_k$) of the system characteristics (P) and the parameter (α_k) can be calculated respectively by Eq. (11).

$$\delta_P = \frac{|\Delta P|}{P}, \delta\alpha_k = \frac{|\Delta\alpha_k|}{\alpha_k} \tag{11}$$

The calculation function $S_k(\alpha_k)$ of sensitivity of the sensitive parameter (α_k) can be obtained based on Eq. (11).

$$S_k(\alpha_k) = \left[\frac{|\Delta P|}{P}\right] / \left[\frac{|\Delta\alpha_k|}{\alpha_k}\right] = \left|\frac{\Delta P}{\Delta\alpha_k}\right| \times \frac{\alpha_k}{P} \quad (k = 1, 2, 3, \ldots\ldots\ldots\ldots n) \tag{12}$$

When the value of $\frac{|\Delta\alpha_k|}{\alpha_k}$ is relatively small, $S_k(\alpha_k)$ can be expressed as

$$S_k(\alpha_k) = \left|\frac{\mathrm{d}f(\alpha_k)}{\mathrm{d}\alpha_k}\right| \times \frac{\alpha_k}{P} \quad (k = 1, 2, 3, \ldots\ldots\ldots\ldots n) \tag{13}$$

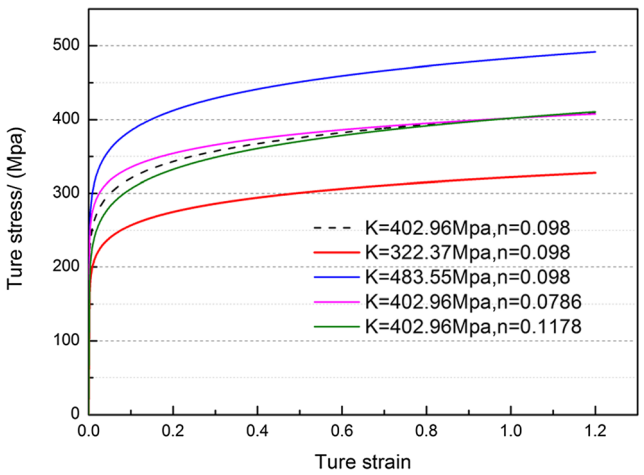

Fig. 14 True stress-strain curve under different values of K and n

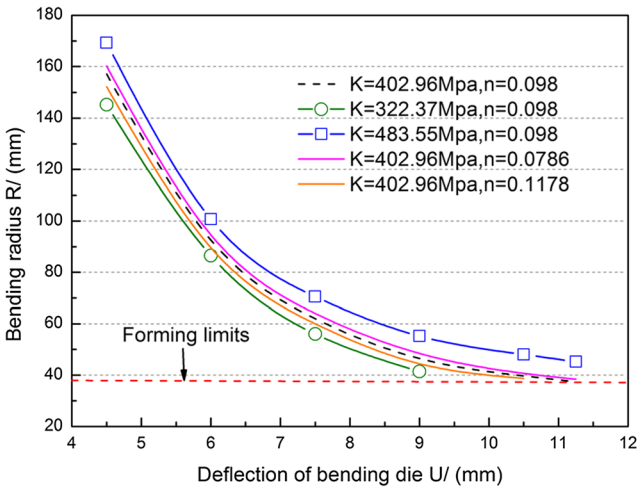

Fig. 15 Effect of intensity coefficient and work-hardening exponent on U-R relationship

Table 2 Range of material parameters in simulation

ρ (kg/m^3)	E/GPa	σ_s/MPa	K/MPa	n
2.136	49.68	200.408	322.37	0.0786
2.403	55.89	225.459	362.67	0.0884
2.67	**62.10**	**250.51**	**402.96**	**0.0982**
2.937	68.31	275.561	443.26	0.1080
3.204	74.52	300.612	483.55	0.1178

Table 3 Sensitivity factors of material parameters on the bending radius

U (mm)	4.5	6	7.5	9	10.5	11.25	Average
S (E*)	0.3461	0.3425	0.3511	0.3529	0.3472	0.3389	0.3465
S (σ_s*)	0.8562	0.8513	0.8576	0.8602	0.8599	0.8624	0.8579
S (K*)	0.2547	0.2671	0.2613	0.2588	0.2523	0.2498	0.2573
S (n*)	0.0864	0.0797	0.0799	0.0835	0.0817	0.0866	0.0830
S (ρ*)	0.0211	0.0199	0.0184	0.0201	0.0214	0.0197	0.0201

The sensitivity factor S_k* of the parameter α_k can be obtained by substituting $\alpha_k = \alpha_k$* into Eq. (13).

$$S_k{}^* = S_k(\alpha_k{}^*) = \left|\frac{df(\alpha_k{}^*)}{d\alpha_k{}^*}\right| \times \frac{\alpha_k{}^*}{P} \quad (k = 1, 2, 3, \ldots\ldots\ldots\ldots n) \tag{14}$$

In which S_k*, $k = 1, 2, 3, \ldots\ldots\ldots n$, is a set of dimensionless non-negative real numbers. If the value of S_k* is increased, the system characteristic P shows more sensitivity to the sensitive parameter α_k* in the reference state.

4.2 Definition of sensitive parameters

According to the method of multiparameter sensitivity analysis described in Section 2, the property of the system characteristic P (tube bending radius after free bending) is mainly affected by the tube material parameters under the constant tube cross section. In this study, the sensitive parameters include density (ρ), modulus of elasticity (E), initial yield stress (σ_s), strength coefficient (K), and strain-hardening exponent (n). The fluctuation ranges of the above parameters are ± 10 and ± 20%, which are shown in Table 2, where the bold line is the baseline state set, the basic material properties of the AA1100 tube.

So as to obtain the sensitivity factors on bending radius of density (ρ), modulus of elasticity (E), initial yield stress (σ_s), strength coefficient (K), and hardening exponent (n), the free-bending process of the AA1100 tube under different deflections of the bending die was simulated using ABAQUS FE code, according to the variation range of each material parameter in Table 2.

Due to less interaction between the factors, only one parameter was changed in the simulation and other parameters were unchanged. Under different deflections of the bending die, the bending radius of the AA1100 tube changes with the variation of the elastic modulus, as shown in Fig. 16.

$$R = f(E)_{U=4.5} = -0.91659E + 221.359 \tag{15}$$

$$S(E)_{U=4.5} = \left|\frac{dR}{dE}\right| \times \frac{E}{R} = \left|\frac{-0.91659E}{-0.91659E + 221.359}\right| \tag{16}$$

The function relation between the bending radius (R) and the modulus of elasticity (E) was established by the method of curve fitting. It is found that the bending radius (R) and the elastic modulus (E) are linearly related and Eq. (15) shows the relationship when the deflection of the bending die is equal to 4.5 mm. Based on Eqs. (13) and (15), the sensitivity function $S_{U=4.5}(E)$ of elastic modulus (E) can be obtained as Eq. (16). The reference value E* = 62.1 GPa is substituted in Eq. (16),

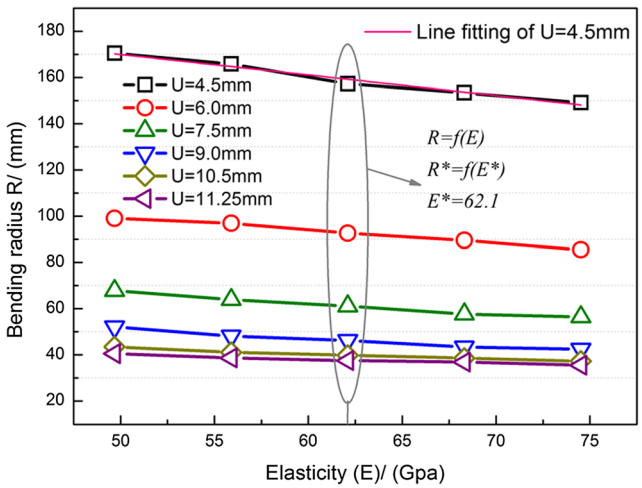

Fig. 16 Bending radius changes with the variation of elastic modulus

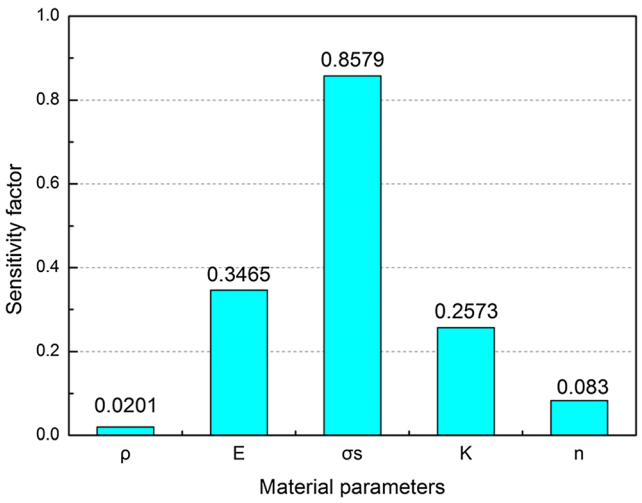

Fig. 17 Average value of sensitivity factors of material parameters on bending radius

Table 4 Comparison of material parameters

Materials	Density ρ (kg/m^3)	Young's modulus E (GPa)	Yield strength σ_s (MPa)	Work-hardening exponent n	Strength coefficient K (MPa)	Bending radius R
Reference material	ρ_0	E_0	σ_{s0}	n_0	K_0	R_0
Target material	ρ_1	E_1	σ_{s1}	n_1	K_1	R_1
Deviation ($D_{\alpha k}$)	D_ρ	D_E	$D\sigma_s$	Dn	D_K	D_R

and the sensitivity factor of the parameter (E) to the bending radius is $S(E*)_{U=4.5} = 0.3461$.

From the above deformation analysis, it can be concluded that the bending radius increases with the decrease of elastic modulus (E), density (ρ), and hardening exponent (n) and the increase of initial yield stress (σ_s) and strength coefficient (K), while Poisson's ratio hardly affects the bending radius. And the analysis procedures of the remaining five material parameters are consistent with the sensitivity analysis of the elastic modulus, and the sensitivity factors of all the material parameters are shown in Table 3 and Fig. 17. According to the sensitivity analysis, the order of sensitivity factors of material parameters on the bending radius in the free-bending process of Al alloy circular tubes is $\sigma_s > E > K > n > \rho$. It is also found that sensitivity factors produced little fluctuations under different deflections of the bending die.

5 *U-R* relationship prediction method

5.1 Calculation method

The *U-R* relationship prediction method was based on the comparison of material parameters (Table 4). And the *U-R* relationship of the target material is obtained by correcting the *U-R* relationship of the reference material according to the comparisons of material parameters. The specific calculation process is as follows:

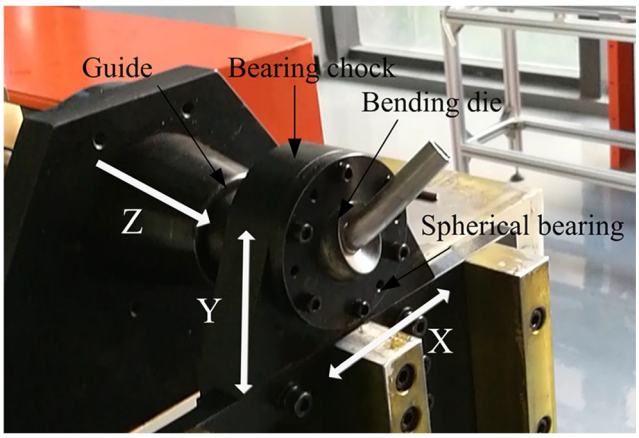

Fig. 18 Bending experiments on the three-axis free-bending equipment

$$\delta(\alpha k)_{(U=X)} = (\pm)\, S\left(\alpha k^*\right)_{(U=X)} \times D_{\alpha k} \tag{17}$$

$$\delta_{(U=X)} = \sum \delta(\alpha k)_{(U=X)} = \sum (\pm) S\left(\alpha k^*\right)_{(U=X)} \times D_{\alpha k} \quad (k = 1, 2, 3, \ldots\ldots\ldots n) \tag{18}$$

$$D_{R(U=X)} = R_{0(U=X)} \times \delta_{(U=X)} \tag{19}$$

$$R_{1(U=X)} = R_{0(U=X)} + D_{R(U=X)} = R_{0(U=X)} \times \left(1 + \delta_{(U=X)}\right) \tag{20}$$

In which the sign (±) depends on the correlation of the parameter (ak) to the *U-R* relationship. Positive correlation takes (+), and vice versa; $\delta(\alpha k)_{(U=X)}$ is the bending radius error (%) caused by the parameter (ak) when the deflection of the bending die is equal to X; $\delta_{(U=X)}$ is the total error (%) of the bending radius that integrated the influence of all parameters with the deflection of the bending die of X.

5.2 Experimental verification

To verify the prediction method, the bending tests for AA6061-T6 tubes were carried out on the three-axis free-bending equipment, as depicted in Fig. 18. Besides, the bending result was compared with the AA1100 tube which was set as the reference material.

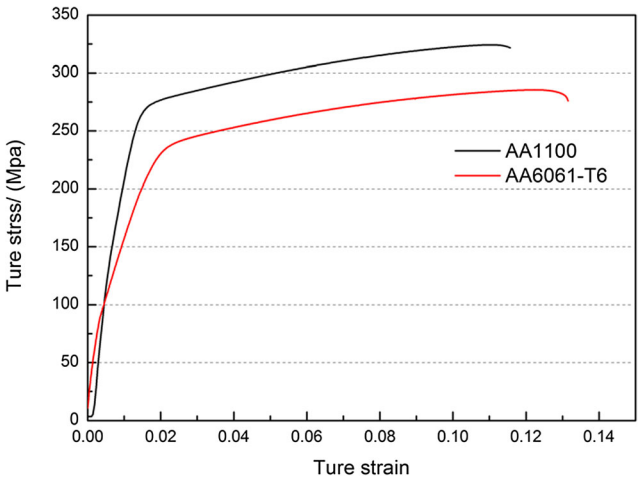

Fig. 19 True stress-strain curve of the AA1100 and AA6061-T6 tubes

Table 5 Comparison of material parameters between the AA1100 and AA6061-T6 tubes

Materials	Density ρ (kg/m^3)	Young's modulus E (GPa)	Yield strength σ_s (MPa)	Work-hardening exponent n	Strength coefficient K (MPa)
AA1100	2.70	62.10	250.5	0.0982	402.96
AA6061-T6	2.73	78.22	234.6	0.1138	365.29
Deviation	1.11%	25.96%	− 6.35%	15.89%	− 9.35%

Figure 19 reveals the comparison between the true stress-strain curve of the AA1100 and AA6061-T6 tubes. Table 5 shows the comparison of material parameters between AA1100 and AA6061-T6 tubes. Since the above two materials belong to the Al alloy, the difference of the density of the material was small. Therefore, the impact of density on *U-R* relationships is ignored. The deviation of Young's modulus, yield strength, work-hardening exponent, and strength coefficient was introduced into the calculation of the deviation of the bending radius. For example, the relative error of Young's modulus of the AA6061-T6 and AA1100 tubes was 25.96% and the sensitivity factor of Young's modulus on the bending radius was 0.3461 when the deflection of the bending die is equal to 4.5 mm; therefore, the deviation of the bending radius caused by Young's modulus can be calculated as Eq. (20). Because the bending radius increases with the decrease of elastic modulus, the actual relative error was equal to − 8.985%. By calculating the deviation of the four parameters, respectively, the total relative error of the bending radius between the AA6061-T6 and AA1100 tubes when the deflection of the bending die is equal to 4.5 mm was obtained of about − 18.09%, and it was easy to know that the bending radius of the AA6061-T6 tube was smaller than the AA1100 tube, as shown in Table 6.

Based on the experimental *U-R* curve of the AA1100 tube, the predicted *U-R* curve of the AA6061-T6 tube was obtained according to the relative error of bending radius of the AA6061-T6 and AA1100 tubes, as described in Fig. 20. It can be found that the predicted *U-R* curve has a good agreement with the experimental *U-R* curve when the deflection of the bending die is relatively large. The deviation of the predicted *U-R* curve and the experimental *U-R* curve may be due to clearance and lubrication conditions which affect a lot when the deflection of the bending die is relatively small.

Table 6 Deviation of the bending radius caused by parameter deviation of the AA6061-T6 tube

	E (%)	σ_s (%)	n (%)	K (%)	$\delta_{(U=X)}$ (%)
U = 4.5 mm	− 8.895	− 5.437	− 1.373	− 2.381	− 18.09
U = 6 mm	− 8.891	− 5.406	− 1.267	− 2.497	− 18.06
U = 7.5 mm	− 9.115	− 5.446	− 1.266	− 2.443	− 18.27
U = 9 mm	− 9.161	− 5.462	− 1.327	− 2.420	− 18.37
U = 10.5 mm	− 9.013	− 5.460	− 1.298	− 2.360	− 18.13
U = 11.25 mm	− 8.798	− 5.476	− 1.376	− 2.336	− 17.99

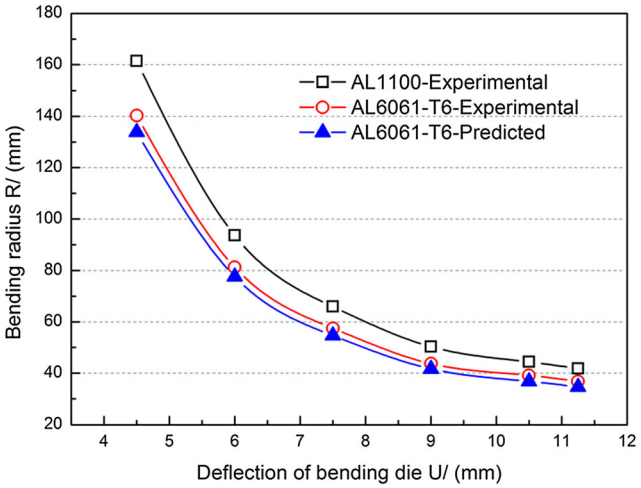

Fig. 20 The predicted *U-R* curve of the AA6061-T6 tube

6 Conclusions

Based on the above deformation analysis, sensitivity analysis, and bending test, the following conclusions can be deduced:

1. For the power hardening aluminum alloy circular tubes, the bending radius (R) increases with the decrease of elastic modulus (E), density (ρ), and strain-hardening exponent (n) and the increase of initial yield stress (σ_s) and strength coefficient (K), while Poisson's ratio hardly affects the bending radius. The variation of deflection (U) of the bending die will not affect the regular pattern.
2. The order of sensitivity factors of material parameters on the bending radius in the free-bending process of power hardening aluminum alloy circular tubes is $\sigma_s > E > K > n > \rho$.
3. The bending test verified the accuracy of the new method to establish the *U-R* relationship of the target power hardening aluminum alloy circular tube based on the material parameter analysis.

Funding information The authors greatly acknowledge the financial support from the National Natural Science Foundation of China (Grant No.51875548), Jiangsu Province Science and Technology Program (Grant No. BE2016156), the Natural Science Foundation of Jiangsu Province (Grant No. BK20151469), the China Aviation Science Foundation (Grant No. 2016ZE52047), and the National Natural Science Foundation International (regional) cooperation and exchange project (Grant No.51711540301).

References

1. Murata M, Kuboki T (2015) CNC tube forming method for manufacturing flexibly and 3-dimensionally bent tubes. Springer, Berlin, pp 363–368
2. Guo X, Jin K, Wang H, Pei W, Ma F, Tao J (2016) Numerical simulations and experiments on fabricating bend pipes by push bending with local induction-heating process. Int J Adv Manuf Technol 84(9):2689–2695
3. Beulich N, Craighero P, Volk W (2017) FEA simulation of free-bending—a preforming step in the hydroforming process chain. J Phys Conf Ser 896:12–20
4. Murata M (1996) Effects of inclination of die and material of circular tube in MOS bending method. Trans Jpn Soc Mech Eng C 62: 3669–3675
5. Guo X, Xiong H, Xu Y, Ma Y, El-Aty AA, Tao J, Jin K (2018) Free-bending process characteristics and forming process design of copper tubular components. Int J Adv Manuf Technol 8:1–17
6. Zhan M, Yang H, Huang L, Gu R (2006) Springback analysis of numerical control bending of thin-walled tube using numerical-analytic method. J Mater Process Technol 177(1):197–201
7. Gantner P (2008) The characterisation of the free-bending technique. Glasgow Caledonian University
8. Gantner P, Harrison DK, Silva AKM, Bauer H (2007) The development of a simulation model and the determination of the die control data for the free-bending technique. Proc Inst Mech Eng B J Eng Manuf 221(2):163–171
9. Gantner P, Bauer H, Harrison DK, Silva AKM (2005) Free-bending—a new bending technique in the hydroforming process chain. J Mater Process Technol 167(2):302–308
10. Ma Y, Xiong H, Wang H, Luo X, Jin K, Xu Y (2017) Simulation and experimental study on three dimensional free bending of complex space elbow. J Net Form Eng 9(2):20–26
11. Guo X, Ma Y, Chen W, Xiong H, Xu Y, El-Aty AA (2018) Simulation and experimental research of the free bending process of a spatial tube. J Mater Process Technol 255:137–149
12. Zhan M, Wang Y, Yang H, Long H (2016) An analytic model for tube bending springback considering different parameter variations of Ti-alloy tubes. J Mater Process Technol 236:123–137
13. Gantner P, Bauer H (2004) FEA—simulation of bending processes with LS-DYNA. 8th international LS-DYNA users conference 2: 33–40
14. Zhou Y, Li P, Li M, Wang L, Sun S (2017) Residual stress and springback analysis for 304 stainless steel tubes in flexible-bending process. Int J Adv Manuf Technol 1:1–9
15. Li H, Yang H, Zhang Z, Li G, Liu N, Welo T (2014) Multiple instability-constrained tube bending limits. J Mater Process Technol 214(2):445–455
16. Zhan M, Huang T, Zhang P, Yang H (2014) Variation of Young's modulus of high-strength TA18 tubes and its effects on forming quality of tubes by numerical control bending. Mater Des 53(3):809–815
17. Li H, Yang H, Song F, Zhan M, Li G (2012) Springback characterization and behaviors of high-strength Ti–3Al–2.5V tube in cold rotary draw bending. J Mater Process Technol 212(9):1973–1987
18. Saltelli A, Annoni P (2000) Sensitivity analysis. Wiley